Analysis of Hydrogen induced Failure in Tensile Tests

Tobias Schaffner[*1], Alexander Hartmaier[2], Thomas Pretorius[1]
[1]thyssenkrupp Steel Europe AG, [2]Ruhr Universität Bochum
*Corresponding author: Kaiser-Wilhelm-Str. 100 - 47166 Duisburg - Germany,
tobias.schaffner@thyssenkrupp.com

Abstract: The focus of this study is to examine damage behavior of ultra-high strength steels (UHSS) in the context of hydrogen transport mechanisms. In order to do this, a combination of representative experiments and physically motivated simulations has been realized. Permeation measurements and slow strain rate tests (SSRT) have been performed in order to determine fundamental material parameters, which were later used for simulation of the material hardening behavior and the hydrogen diffusion behavior. Corresponding three-dimensional simulations were performed using the structural mechanics module of COMSOL Multiphysics. Local stress and strain fields combined with hydrogen concentration allow a physical estimation of the critical fracture areas, whereas local hydrogen contents were predicted using time dependent hydrogen transport model Thus a better understanding of the hydrogen influence on the fracture behavior has been achieved.

Keywords: hydrogen transport, slow strain rate test, ultra-high strength steel, hydrogen embrittlement, FEM Simulation

1. Introduction

In the course of the overall vehicles weight reduction, the development of advanced high strength steel concepts gains in importance. Especially UHSS concepts like martensitic steel grades are future-oriented. Due to their high strength properties combined with an outstanding crash performance, the production of thin safety components is enabled.

However, as examined in various reports high strength steel grades can exhibit a high vulnerability to hydrogen embrittlement (HE) [1]. In addition to various possibilities for hydrogen absorption during steel production or usage, the main reason for HE vulnerability is the complex microstructure. Several structural features like dislocations, grain and phase boundaries, carbides and precipitates can trap hydrogen temporary. Thus the overall rate of hydrogen diffusion of UHSS grades is generally some orders of magnitude lower than of pure iron. These structural effects in combination with non-homogenous stress distributions and plastic deformation lead to local hydrogen accumulation and promote material failure.

Macroscopic prediction of the hydrogen induced failure is a key factor to secure the industrial usage of UHSS components. In order to do so, the material dependent hydrogen diffusivity was investigated in permeation measurements. In addition slow strain rate tests (SSRT) of tensile specimens under varying hydrogen content were performed to characterize the forming process. The time dependent tensile straining was simulated using the structural mechanics application of COMSOL Multiphysics. A physically motivated, macroscopic hydrogen transport model was implemented to illustrate the hydrogen repositioning process. Thus the simultaneous calculation of the time-dependent stress field and the local hydrogen concentration was realized. Finally critical component areas defined over hydrostatic stress gradients, plastic strain and the hydrogen concentration were localized.

2. Model for Hydrogen Diffusion in Steel

The transport behavior of hydrogen in UHSS grades is driven by several effects. The hydrogen diffusion flux is induced by the gradient of the chemical potential, which depends on the hydrogen distribution in lattice and various stresses. External or residual stresses affect hydrogen fluxes by generating hydrostatic stress gradients. Tensile hydrostatic stresses extend the volume of the interstitial lattice sites, whereas compressive stresses lead to the lattice sites volume reduction. As a consequence dissolved hydrogen atoms tend to move to areas of tensile hydrostatic stress.

The hydrogen diffusion flux J driven by stress and concentration gradients is given by the following equation [2].

$$J = -D\nabla(c_L) + Dc_L \frac{V_H}{RT}\nabla(\sigma_h) \qquad (1)$$

In this equation D denotes material dependent lattice diffusivity while c_L represents concentration of hydrogen in lattice sites. The parameter $V_H = 2{\cdot}10^{-6}$ m³/mol represents partial molar volume of hydrogen in α-iron at temperature $T = 293$K and the parameter $R = 8.3141$ J/molK represents the universal gas constant. Hydrostatic stress is denoted as σ_h.

Mass conservation requires that the total hydrogen concentration c_{tot} in a body of the volume V is equal to the flux of hydrogen through the body's surface S. Accounting to this by usage of the divergence theorem we gain a general diffusion equation.

$$\frac{\partial c_{tot}}{\partial t} = D\nabla^2(c_L) - Dc_L \frac{V_H}{RT}\nabla^2(\sigma_h) \qquad (2)$$

In addition to hydrogen in interstitial lattice sites hydrogen can also be caught by an amount of material defects, called hydrogen taps. Therefore the total concentration of hydrogen is defined by the sum of trapped hydrogen concentration c_T and the lattice hydrogen concentration c_L [3].

$$c_{tot} = c_L + c_T \qquad (3)$$

Hydrogen transport between the trap sites can be neglected. As proposed by Oriani the hydrogen in lattice sites and the hydrogen in trap sites are in chemical equilibrium [4]. Assuming a low hydrogen trap occupancy the lattice diffusivity D can be replaced by an effective hydrogen diffusivity D_{eff}. In this case the hydrogen concentration in trap sites can be expressed as a function of the lattice hydrogen concentration.

$$c_T = \frac{N_T}{1 + (K_T c_L / N_L)^{-1}} \qquad (4)$$

In this equation K_T denotes trap equilibrium constant. The trap density N_T depends on the plastic deformation ε_{pl}. Several researchers investigated the relation between the trap density and the plastic strain. Sofronis and McMeeking [5] fitted one of these investigations examined by Kumnick and Johnson [6] for pure iron. Assuming that the changes in the trap density due to plastic deformation of pure iron are comparable to these of UHSS we can define the trap density as follows.

$$\log N_T = 23.3 - 2.33e^{-4e_{pl}} \qquad (5)$$

Substituting (2), (3) and (4) we gain the final hydrogen diffusion equation for the hydrogen transport behavior in steel used in this study.

$$\left(1 + \frac{\partial c_T}{\partial c_L}\right)\frac{\partial c_L}{\partial t} = D_{eff}\nabla^2(c_L) - D_{eff}c_L \frac{V_H}{RT}\nabla^2(\sigma_h) \qquad (6)$$

3. Material and Methods

3.1 Material

Experimental investigations of this study were performed on a laboratory-prepared multiphase UHSS grade of the thyssenkrupp Steel Europe AG. The material was prepared as uncoated hot-rolled steel sheets with a thickness of 1.5 mm. The microstructure of this concept steel shows only martensitic phases. The characteristic mechanical values examined by tensile tests and further important material data are summarized in table 1. In the following the concept is referred to as 1200M.

Table 1: Material data for 1200M

Property	Symbol	Value
yield strength	R_p	1090 MPa
tensile strength	R_m	1250 MPa
Young´s modulus	E	200 GPa
Poisson´s ratio	ν	0.3
fracture strain	A	6.5
density	ρ	7850 kg/m³

3.1 Characterization of Hydrogen Transport by Permeation Measurements

The hydrogen transport behavior of the investigated UHSS grade has been analyzed by permeation measurements according to DIN EN ISO 17081 [7]. At first, specimens of 1200M were machined to dimensions of 60 x 60 mm. The specimen surfaces were ground and polished to a thickness of 1 mm. The permeation measurements were performed in a Devanathan double-cell setup, consisting of a charging cell and an oxidation cell separated by the steel sample. The charging cell is filled with a 0.025 % NH_4SCN aqueous solution, while the oxidation cell contains 0.1 M solution of NaOH. The area of the sample exposed to the electrolytes in both chambers was 9.6 cm². The current density was set to 0.5 mA/cm² and all tests were performed at room temperature (293 K).

The process of galvanostatically charging provides a constant hydrogen concentration on the sample surface in the charging cell. After adsorption followed by absorption, the hydrogen atoms diffuse through the sample and release on the opposites sample surface. The resultant permeation current I_P can be detected by oxidation of the released hydrogen atoms. The corresponding hydrogen permeation flux J_P can be identified as follows:

$$J_P(t) = \frac{I_P(t) \cdot A}{F}, \tag{7}$$

where A and F denote the sample surface area exposed to the oxidation cell and the Faraday´s constant. The effective hydrogen diffusivity D_{eff} can be calculated by the time-lag parameter t_L (time at $0.63 \cdot J_{Pend}$) and the sample thickness L.

$$D_{eff} = \frac{L^2}{6 \cdot t_L} \tag{8}$$

3.2 Characterization of Hydrogen induced Failure Behavior by Slow Strain Rate Tests

Slow strain rate tests with a constant displacement speed v of $1 \cdot 10^{-4}$ mm/s were performed to characterize the fracture behavior with respect to different hydrogen charging conditions [8]. The experimental setup and the chosen specific shear tensile specimen geometry, are shown in figure 1. Further, the SSRT-setup is shown in top of figure 1.

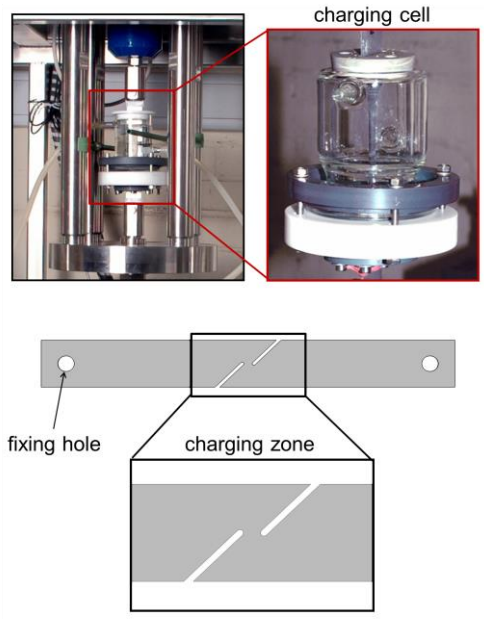

Figure 1. Experimental setup and specimen geometry for SSRT.

In order to investigate different hydrogen contents, the specimens were charged electrochemically before SSRT. The charging time was set to 80 minutes to ensure a homogenous hydrogen saturation. Basically, the specimens were charged in an additional cell filled with the aqueous solution 0.025 % NH_4SCN. The examined cathodic current densities were set to 0.01 and 0.75 mA/cm² in order to realize different initial hydrogen concentrations.

After specimen failure one half of the sample was prepared for fracture analysis. Scanning electron microscopy (SEM) was used to characterize fracture surfaces. The fracture direction was recorded by light microscopy (LM).

4. Simulation of SSRT by COMSOL Multiphysics

The *Solid Mechanics* application mode was used to simulate the straining process with respect to hydrogen content. For this a 3D

component of the shear specimen geometry was generated. The model was computed by a *Time dependent solver* in range of the experimental SSRT to consider the time dependent process of hydrogen transport. In order to optimize numeric efficiency the model was reduced to the charging zone of the specimen (figure 2).

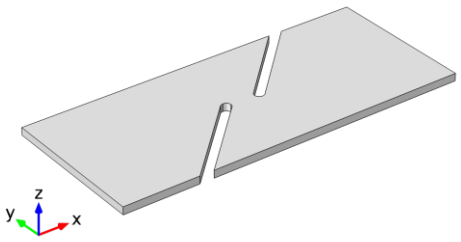

Figure 2. SSRT simulation domain.

4.1 Boundary Conditions

Several *Boundary Conditions* were applied to represent the SSRT. The charging cell surrounding the specimen while testing was defined by a *Roller* condition. Further, the straining process was represented by a *Prescribed Velocity* condition on the front side of the sample. The applied velocity value was estimated from the experimental displacement speed *v*.

Figure 3 summarizes all used boundary conditions for the straining simulation.

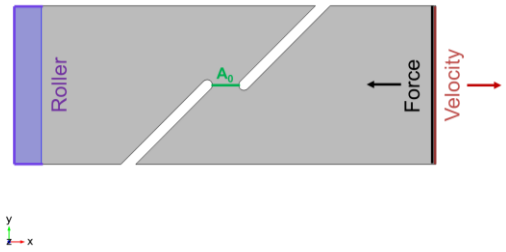

Figure 3. Mechanical boundary conditions.

To compare the experimental and simulation results of the SSRT a global tension stress was calculated. Therefore the reaction force *solid.RF* on the front side of the sample was calculated and related to the initial specimen cross section A_0. The resultant numeric tension stress was compared to the experimental stress-time curve.

4.2 Meshing

A quad mesh following Figure 4 was composed by the *Swept* mesh node. The element size parameters were selected following table 2. The parameters enable an increasing refinement for the resolution of narrow regions. In order to consider thickness dependent material behavior the number of elements in z direction was set to 5 and the total number of elements was 7750.

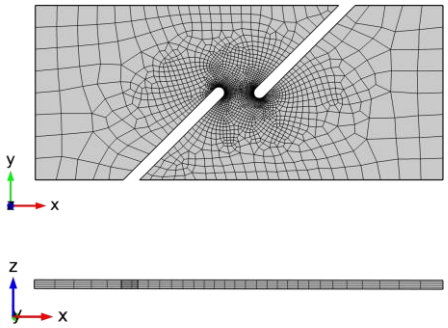

Figure 4. SSRT simulation mesh.

Table 2: Mesh data for 1200M

Parameter	Value
maximum element size	5E-2
minimum element size	7E-6
maximum element growth rate	1.1
curve factor	0.26
resolution of narrow regions	2

4.3 Plasticity Modelling

Plasticity was considered by adding the sub-node to the *Linear Elastic Material* node of the *Solid Mechanics* interface. Assuming isotropic material hardening behavior the von Mises yield function F was defined following equation 9, where σ_{Mises} and σ_{ys} denote the von Mises stress and the yield level.

$$F = \sigma_{Mises} - \sigma_{ys} \tag{9}$$

The yield level is defined as the sum of the initial yield level σ_{ys0} and the hardening function σ_h. A user specific hardening function was derived from the experimental true stress - true strain dependency for 1200M. All other required data is summarized in table 1.

4.4 Modelling of Hydrogen Diffusion

The time dependent diffusible hydrogen concentration σ_L, as proposed in equation 6, was implemented by addition of a *General Form PDE* node. A three dimensional hydrogen distribution in the sample was considered by means of the *Conservative Flux Vector* following equation 10.

$$\Gamma = -D_{eff}\nabla c_L - D_{eff} c_L \frac{V_H}{RT}\nabla \sigma_h \qquad (10)$$

The effective diffusion coefficient D_{eff} was s according to section 3. Further, the time derivative for total hydrogen concentration was defined by the *Damping Coefficient* d_a following equation 11.

$$d_a = 1 + \frac{c_T}{c_L}\left(1 - \frac{c_T}{N_T}\right) \qquad (11)$$

Boundary and initial conditions were adapted according to the experimental charging process. An initial lattice hydrogen concentration c_{L0} was defined by solving the nonlinear system of equation 3 for given initial total hydrogen concentrations c_{tot0}. In order to calculate c_{L0} the equations of the trap density and the trap concentration were implemented by *Analytic Function* nodes. Additionally a *Dirichlet Boundary Condition* with a constant hydrogen concentration was used to consider the permanent charging procedure. The value for the boundary concentration was determined by experimental permeation measurements.

In figure 5 all used conditions for the hydrogen charging process are summarized.

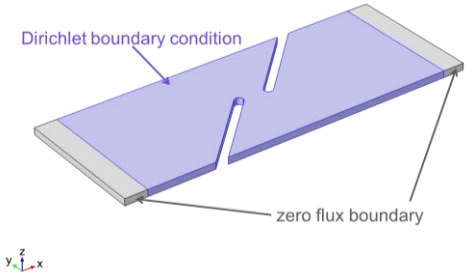

Figure 5. Boundary conditions for *PDE*.

5. Results and discussion

The measured stress-time curves for the two charging variants and the calculated tension stress, according to section 4.1, are shown in figure 6.

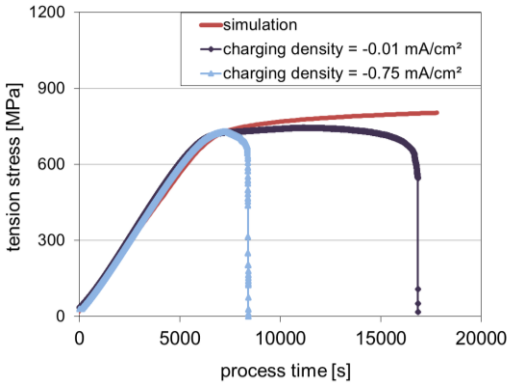

Figure 6. Measured and simulated tension stress.

Comparing the stress evolution of the experimental curves, it can be seen that the global time to failure is strongly affected by the current density. The specimen charged with a density of 0.75 mA/cm² fractures more quickly at a lower displacement level. In contrast, the specimen charged with a density of 0.01 mA/cm² fractures more slowly at higher displacement levels.

The charging process also affects fracture on the microscopic and macroscopic scale. In Figure 7 the fracture surfaces of the SSRT specimens is shown.

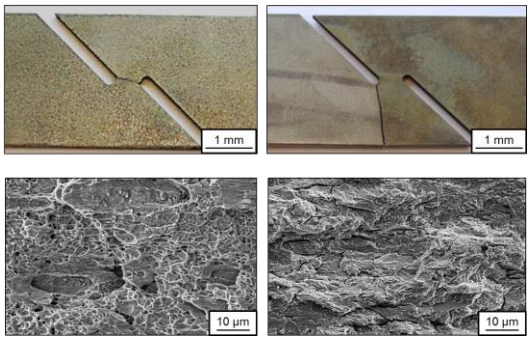

Figure 7. Direction of crack (top) and the fracture surfaces (bot) for current density of 0.01 mA/cm² (left) and 0.75 mA/cm² (right)

At the lower current density the specimen shows a ductile shear fracture without any signs of brittle material behavior. The crack propagation occurs between the shearing slots in longitudinal direction. In contrast, for the higher current density the fracture surface shows a clearly brittle area. Further, the crack initiates at one of the shearing slots and propagates in transverse direction towards the cutting edge. These results confirm the assumption that the damage behavior in SSRT can be changed by the charging process. Differences in the crack initiation and propagation behavior indicate that the cause of damage strongly relates to the hydrogen content.

In order to investigate failure sources the *Solid Mechanics Simulations* were used. Therefore critical parameters like the effective plastic strain (*solid.epe*), the hydrostatic stress (*solid.pm*) and the diffusible hydrogen content (c_{tot}) were analyzed. The simulation results are compared in figure 8 and 9 for both charging variants.

Comparing the simulation results it becomes clear that the distribution of the total hydrogen concentration strongly depends on plastic strain state and hydrostatic stress gradients.

In case of the lower current density (figure 8) the simulation shows a significant high plastic deformation between the shearing slots in time of failure. In contrast, the initial concentration of hydrogen is comparatively small. Combining these conditions, the diffusible hydrogen is driven to concentrate between the shearing slots.

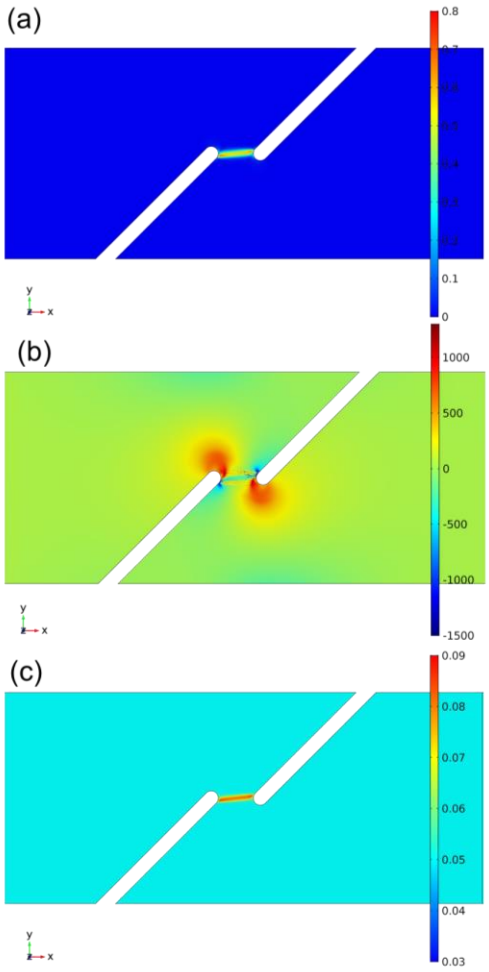

Figure 8. Effective plastic strain (a), hydrostatic stress (b) and diffusible hydrogen content (c) for 0.01 mA/cm² at time of failure

In case of the higher current density (figure 9) the simulation shows a lower state of plastic strain at time of failure. The highest values for the hydrostatic tensile stress are on the top of the shearing slots. Based on the extended volume of the interstitial lattice sites hydrogen atoms are driven to accumulate in this area. Consequently a critical combination of conditions is reached and result in a premature abruptly failure.

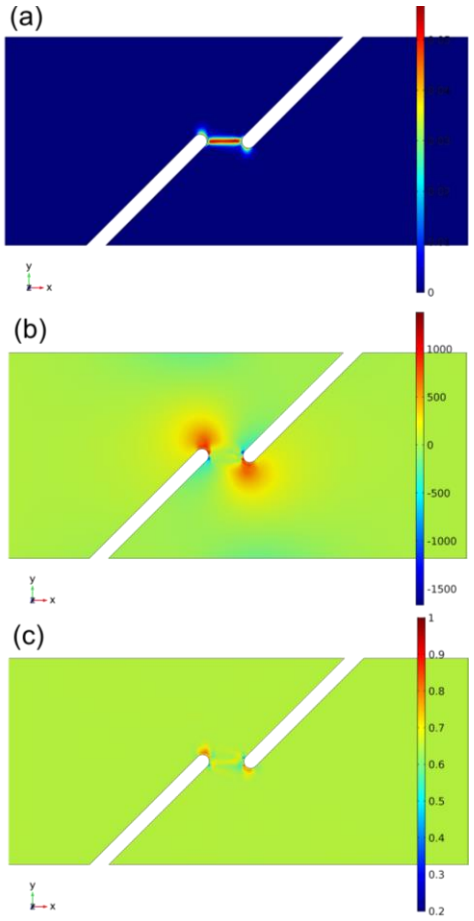

Figure 9. Effective plastic strain (a), hydrostatic stress (b) and diffusible hydrogen content (c) for 0.75 mA/cm² at time of failure

6. Conclusions

The hydrogen induced damage behaviour of the UHSS grade 1200M was examined by means of representative experiments and physically based simulations.

A time dependent hydrogen transport model was implemented for analysis of the possible failure sources. It has been shown that the critical fracture areas can be localized only if all crucial parameters are taken into account. Simulations performed using COMSOL Multiphysics deliver a very good agreement with experimental data on crack initiation area and crack propagation direction.

Failure prediction by implementing damage models is a subject of the further studies.

7. References

[1] J. Rehrl: Mechanical properties and fracture behavior of hydrogen charged AHSS/UHSS grades at high- and low strain rate tests, Journal of Materials Science & Engineering, Volume 590, (2014)

[2] S. Serebrinsky: A quantum-mechanically informed continuum model of hydrogen embrittlement, Journal of the Mechanics and Physics of Solids, Volume 52, pp.2403-2430 (2004)

[3] A.H.M. Krom: Hydrogen transport near a blunting crack tip, Journal of the Mechanics and Physics of Solids, Volume 47, pp.971-992 (1999)

[4] R. A. Oriani: The diffusion and trapping of hydrogen in steel, Acta Metallurgica, Volume 28, pp.33-39 (1970)

[5] P. Sofronis: Numerical analysis of hydrogen transport near a blunting crack tip, Journal of the Mechanics and Physics of Solids, Volume 37, pp.317-350 (1989)

[6] A.J. Kumnick: Deep trapping states for hydrogen in deformed iron, Acta Metallurgica, Volume 28, pp.33-39 (1980)

[7] ISO 17081: 2014, Method of measurement of hydrogen permeation and determination of hydrogen uptake and transport in metals by an electrochemical technique

[8] ISO 7539-7:2005, Method for slow strain rate testing

8. Acknowledgements

The author would like to thank Dr. Kirill Khlopkov and Dr. Valentin Kokotin for their helpful advices in various issues examined in this paper. Sincere thanks are also due to Wolfgang Arendt, Dr. Thomas Lostak and Norbert Rössler for the execution of several experimental investigations.